Adaptive Behavior

Power Efficient Adaptive Behavior through a Shape Changing Elastic Robot

Journal:	*Adaptive Behavior*
Manuscript ID	AB-20-0050.R3
Manuscript Type:	Article
Date Submitted by the Author:	n/a
Complete List of Authors:	Katiyar, Shiv; Monash University - Malaysia Campus, Gouwanda, Darwin; Monash University - Malaysia Campus Iida, Fumiya; Cambridge University Nurzaman, Surya Girinatha; Monash University - Malaysia Campus,
Keywords:	Shape Adaptation, Power Efficient, Behaviors, Elastic Structure, Soft Robots
Abstract:	The adaptive morphology of a robot, such as shape adaptation, plays a significant role in adapting its behaviors. Shape adaptation should ideally be achieved without considerable cost, like the required power required to deform the robot's body, and therefore it is reasonably considered as the last resort in classical rigid robots. However, the last decade has seen an increasing interest in soft robots: robots that can achieve deformability through their inherent material properties or structural compliance. Nevertheless, the dynamics of this type of robots is often complex and therefore it is difficult to substantiate whether the cost like the required power for changing its shape will be worthwhile to achieve the desired behavior. This paper presents an approach in the development and analysis of a shape-changing locomoting robot, which relies on the ability of elastic beams to deform and vibrate. Through a proper use of elastic materials and the robot's vibration based dynamics, it will be shown both analytically and experimentally how shape adaptation can be designed such that it leads to desirable behaviors, with better power efficiency compared to when the robot solely relies on changing its control input. The results encourage emerging direction in robotics that investigates approaches to change robots' behaviors through its adaptive morphology.
Note: The following files were submitted by the author for peer review, but cannot be converted to PDF. You must view these files (e.g. movies) online.	
AB_Vid_Rev.mp4	

Power Efficient Adaptive Behavior through a Shape Changing Elastic Robot

Shiv A. Katiyar [1], Darwin Gouwanda [1], Fumiya Iida [2] and Surya G. Nurzaman[1,*]

[1] School of Engineering, Monash University, Malaysia
[2] Bio-Inspired Robotics Laboratory, University of Cambridge, United Kingdom
* Correspondence: surya.nurzaman@monash.edu;

Abstract: The adaptive morphology of a robot, such as shape adaptation, plays a significant role in adapting its behaviors. Shape adaptation should ideally be achieved without considerable cost, like the required power required to deform the robot's body, and therefore it is reasonably considered as the last resort in classical rigid robots. However, the last decade has seen an increasing interest in soft robots: robots that can achieve deformability through their inherent material properties or structural compliance. Nevertheless, the dynamics of this type of robots is often complex and therefore it is difficult to substantiate whether the cost like the required power for changing its shape will be worthwhile to achieve the desired behavior. This paper presents an approach in the development and analysis of a shape-changing locomoting robot, which relies on the ability of elastic beams to deform and vibrate. Through a proper use of elastic materials and the robot's vibration based dynamics, it will be shown both analytically and experimentally how shape adaptation can be designed such that it leads to desirable behaviors, with better power efficiency compared to when the robot solely relies on changing its control input. The results encourage emerging direction in robotics that investigates approaches to change robots' behaviors through its adaptive morphology.

Keywords: Shape Adaptation; Power Efficient; Behaviors; Elastic Structure; Soft Robots.

1. Introduction

By observing examples from living and artificial systems, it has been shown that morphology plays a significant role in their behavior [1–4]. In robotics, behavior is commonly defined as the robot's dynamics resulting from the interaction among its control input, body morphology and environment [3,4]. Recently, the importance of adaptive morphology, such as shape adaptation, is also emphasized as an emerging design principle that can extend dynamic performances which may lead to different behaviors and even contributes to added functionalities [5–7].

Nevertheless, one of the main challenges in shape adaptation is the need of materials or structures that can be deformed easily without considerable cost, such as the power required by the robots to deform them [8,9]. It is therefore reasonable that shape adaptation in classical rigid robots is commonly considered as the last resort or may not even be considered at all, and most of them reasonably rely on their control input to adapt their behavior. Classical examples of shape adaptation in robots made of rigid materials are modular robots, where different rigid modules controlled by dedicated planners are able to reshape themselves to adapt their behaviors and functionalities [5, 10–13]. Nevertheless, due to the use of rigid components, modular robots are primarily used as proof of concept due to the mechanical complexity and high-power requirements [5].

In this regard, the last decade has seen a lot of interests in robots at least partially made of soft, deformable and elastic materials, commonly referred to as soft robots [8,9,14–18]. Due to the ability to flexibly deform, it is expected that the robots can be more adaptable, energy efficient and safer to use than the conventional rigid material robots. When it comes to soft robots, it is proposed that the key word is deformation [8,9]. In soft robotics, deformation can be achieved through inherent material compliance such as elastic bag filled with granular matter [19,20] or fluid driven elastomers (21; 22) as well as structural compliance like tensegrity structures [23, 24] or deformable elastic beams

[25–27]. Some of the applications of soft robots include grippers [19; 21; 28] assistive wearable devices [29; 30], medical robotics [31; 32] and locomotion [20; 22; 23; 25; 27; 36]. In terms of locomotion, in more details, different mechanisms have been investigated in the last few years including those driven by jamming mechanism[20], pneumatic based actuation [22], tensegrity structures[23; 24; 33–35] as well as vibration induced locomotion [25–27; 36].

One of the most important features of soft robots is its potential shape adaptation ability. In soft robotics, shape adaptation has been investigated based on various approaches like origami, tensegrity structure, adhesive materials and growing soft robots (37–41). Nonetheless, among all the approaches, none of them attempts to quantify the balance between the cost for changing the shape, such as the required power or energy, and whether it results in the desirable behavior. Aside from shape adaptation, another active area where adaptive morphology is investigated is stiffness adaptation. Here, for example, the stiffness of the robot can be varied under certain stimuli such as temperature, electric or magnetic fields, and pressure (42–45).

From fundamental perspectives, there are studies that focus on demonstrating that complex control problems can be simplified by an appropriate choice of morphology such as in locomotion (46–48) or grasping (19; 21). The result, along with the possibility to adapt a robot's behavior through adaptive morphology, leads to proposals of fundamental concepts to explain how both control and morphology affect a robot's behavior (49–51). One of the latest proposals is known as the concept of control morphology (CM) space as shown in Fig. 1 (50). The concept emphasizes that if a robot can change its morphology, such as shape, then it can adapt the behavior by either changing its morphology, control input, or both. The term control input, such as motor control input, noticeably means the common control input used to change the robot's behavior assuming that it is notable to change its morphology.

As previously explained, shape adaptation in classical rigid robots is reasonably considered as the last resort or may not even be considered at all. In other words, from the perspective of CM space,

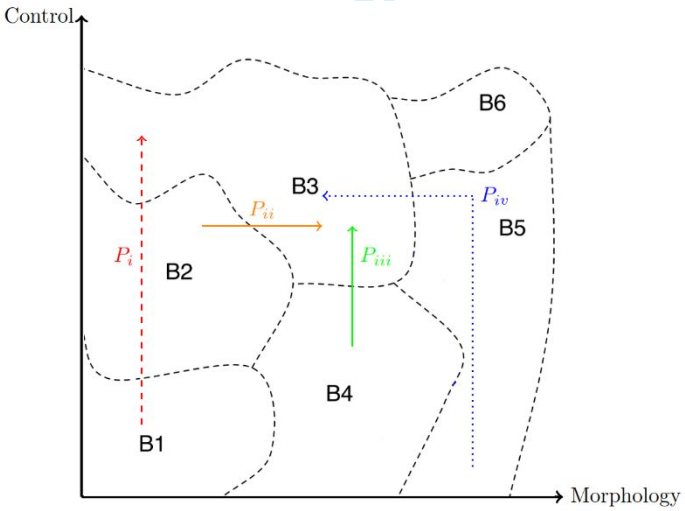

Figure 1. The motivation of this research based on the concept of Control-Morphology (CM) space proposed in (51). B1 until B6 show particular behaviors of a robot depending on the control input given to the robot and its morphology such as shape. The path P_i-P_{iv} show the path taken in CM space to reach a particular behavior. Based on the concept, it can be seen that as traditional rigid body robots generally have a fixed morphology or require high cost such as the required power to change their morphology, the behaviors generally lie on a fixed point on morphology axis and moves along the control-space(e.g. path Pi or P_{iii} representing rigid robot (52; 53)). On the other hand, as it may be less costly for soft robots to adapt its morphology, it should have more flexibility to travel the CM space by either changing the control input (e.g. path P_i or P_{iii}),morphology (e.g. path P_{ii} representing shape-changing robots such as origami robots (37; 38)) or both (e.g. path P_{iv} (6; 54))

the robots commonly take the vertical paths, P_i and P_{iii}, shown in Fig. 1. However, soft robots with compliant body, either based on inherent material properties or structural compliance, may take other paths shown in the figure through shape adaptation. Nevertheless, the dynamics of robots made of soft and elastic materials is commonly quite complex due to its deformability and compliance (8). Therefore, it is difficult to substantiate whether the cost to perform shape adaptation, such as the power required, will be worthwhile to achieve the desired behavior. Moreover, referring to Fig. 1, it's intriguing to quantify and see whether taking the horizontal paths, i.e. changing the shape, in soft robots will be worthwhile in terms of cost such as power required compared to taking the vertical ones, i.e. changing the control input.

This paper presents an approach in the development and analysis of a shape-changing locomoting robot, which relies on the ability of elastic beams to deform and vibrate. The robot is elastic, easy to develop, low in cost, light in weight and can be developed easily by using commercially available. The robot can also be actuated by a single motor, meaning that it only requires one control input which will ease the analysis. Moreover, as the deformability of the robot relies on a structural compliance of elastic beams, the deformation may not be as complex of robots made of softer materials, which will also make the analysis easier. It will be shown that due to the use of elastic materials, the required power to change the robot's shape will not be significant. On the other hand, through a proper characterization of the vibration-based nature of the robot's motion, the robot can be designed such that shape adaptation will lead to different desired behaviors. In other words, it will be shown both analytically and experimentally how shape adaptation can be designed such that it leads to desirable behaviors with better power efficiency, compared to when the robot solely relies on changing its control input to achieve them.

The rest of the paper will be organized as follows. In the second section, the basic concept and mathematical model of the robot will be explained including how it can be used to characterize the robot's behaviors and the required power to change them. The third section explains the developed robot and experimental setup, while fourth section explains the experimental results that focus on the analysis of the required power to change the behavior of the robot by changing its shape and control input. Finally, the conclusion will be made in the last section along with possible future works.

2. Basic Concept and Relevant Mathematical Model

The structure of the developed robot can be explained by Fig. 2 and made of elastic beams. The mass of the foot and the mass of the curved beam is negligible when compared to the mass of motors placed at the center point of robot body. Thus, we model the dynamics of the robot based on this figure as a mass spring system. Due to the use of elastic material to form its body, it is assumed that the robot can change its shape to two extreme configurations as also shown in the Fig. 3. The first one is referred to as upright position, while the second one is flat position. Because the shape resembles an inverted U-shaped curve and the robot will be mainly made of elastic beam, from this point onward, it will simply be called Inverted U-Shaped Curved Beam Robot (IUCBR). From application point of view, the robot is designed with the particular shape such that it will be straight forward for the robot to

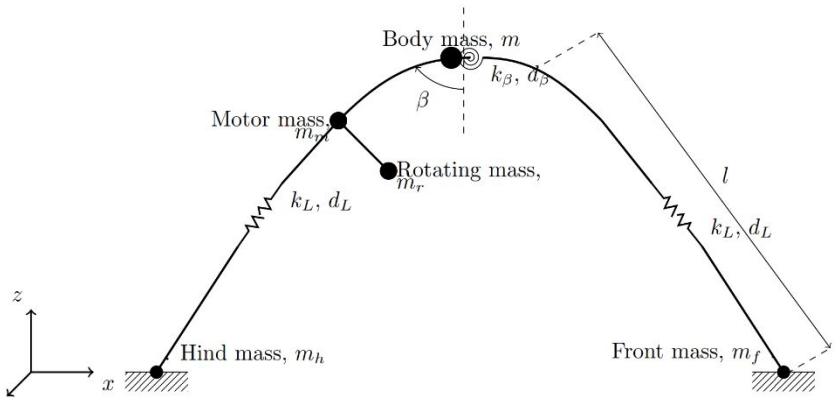

Figure 2. Equivalent schematic diagram of the physical robot used in this paper.

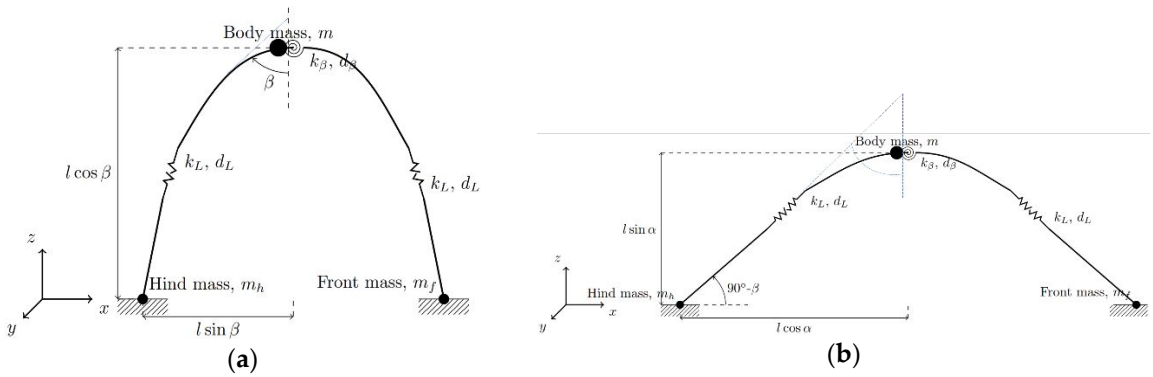

Figure 3. A simplified version of the schematic diagram of inverted U-shape curved beam robot in the two of its configuration used for the purpose of mathematical modelling. (a) β the angle between the robot body and the vertical, being ≈ 30° referred as the upright position. (b) And, (90° – β), the angle between the robot leg and horizontal is ≈ 60° being referred to as flat position.

deform and change its shape to travel in con spaces, a common challenge in studies on soft robot locomotion (20; 22). It is therefore reasonable to see whether it is possible to have different behaviors that are more suitable to deal with normal or confined spaces through the robot's shape changing ability, with the assumption that the required power to change the shape can be minimized due to the use of elastic materials.

In terms of modeling, for the sake of simplicity, we assume that the robot structure has negligible foot and curved beam mass as compared to the mass of motors that will be placed on the robot body. Also, lumped mass concentrated at a single point is assumed instead of distributed mass of different parts. As shown in Fig. 3, the mass of hind foot and front foot m_h and m_f are assumed to be concentrated at the middle and lowest most point of the robot legs. k_L and d_L represent the longitudinal springs stiffness and damping coefficients of the elastic material strips used to make the robots legs. Similarly, k_β and d_β symbolizes the elastic beam torsional spring stiffness and damping coefficient respectively. As mentioned in previous research (25), for the sake of simplicity d_β can be neglected.

The mass of the robot, which may include instrumentation required to change the shape of the robot and collect experimental data, is indicated by body mass, m, and is approximated to be located at the centre and topmost position of the robot body. l refers to the leg length that is considered to makes an angle with a vertical line at the top of the robot. Fig. 3a shows IUCBR in upright position and it is assumed that angle $\beta \approx 30°$ while for other configuration shown in Fig 3b that angle $(90° - \beta) \approx 60°$.

All in all, the equivalent mass spring model of the robot shown in Fig. 3 is analyzed with the following assumptions for linearization and simplicity:

1. The wide feet of the robot are sufficient to balance the curved beam robot in frontal plane thus we focus primarily on the locomotion in the sagittal plane. In other words, the motion is only considered along the x and z axis shown in Fig. 3.
2. The combined mass of DC and servo motor is approximated at the top centre point while robot foot mass is at the bottom of the leg.
3. The linear and rotating ability of the elastic material is represented by longitudinal and torsional spring element placed at their dominant spots i.e. at the midpoint of the legs and at the centre top point of the body respectively.
4. The longitudinal and the torsional stiffness coefficients as mentioned in the previous assumption are linear and constant irrespective of the motion of the curved beam robot.

The key assumption related to the change of the expected behavior based on the design and shape changing ability is the difference of the resonance frequencies of the robot in different shape. Resonance frequency is a well-known concept in vibration dynamics which states that the induced vibration in a structure will show a distinct motion with large amplitude if the frequency that causes the vibration matches the natural frequency of the structure (25). As will be shown, the motion of the robot will be explained based on two resonance frequencies, denoted as torsional and longitudinal ones, whose

values will change due to the change of the robot's shape. The longitudinal oscillations will cause the robot to swing back and forth in the sagittal plane along x axis while torsional oscillations will generate distinct up and down hopping in sagittal plane along z axis (25). Because of the distinct motion driven by different resonance frequencies at different shapes, it is hypothesized that the change of the robot's shape can lead to the desired behavior in the context of moving in a vertically confined space. On the other hand, it is also assumed that the power required to change the shape will not be high due to the elasticity of the robot body. In relation to the assumptions, the next two sub-chapters will discuss deeper on the relationship between the two resonance frequencies and the robot's shapes. Here, for the sake of simplicity, it is also assumed that when IUCBR in upright position the angle β approximately equals to 0°, while for the flat configuration, the angle β is assumed to be 90°.

As derived in the appendix, for the upright and flat configuration the torsional resonance frequencies are as follows, where the subscript *UT* stands for upright torsional and *FT* stands for flat torsional:

$$\omega_{UT} = \sqrt{\frac{2k_\beta - mgl}{ml^2}} \qquad \omega_{FT} = \sqrt{\frac{2k_\beta + mgl}{ml^2}} \tag{1}$$

Furthermore, the longitudinal frequency for both the configuration is defined as follows where the subscript *UL* and *FL* refer to upright longitudinal and flat longitudinal respectively,

$$\omega_{UL} = \omega_{FL} = \sqrt{\frac{2k_L}{m}} \tag{2}$$

From the detailed mathematical model described in the Appendix section it is noticeable and later supported with experimental results, that we can vary the locomotion behavior of the robot by changing the configuration, i.e. shape of the robot. By observing equation 1, 2, 3 and 4, assuming that the torsional resonance frequency is larger than the longitudinal one, it is indicated that the two resonance frequencies will be closer to each other when the robot is in the upright configuration compared to when it is in the flat one. On the other hand, the opposite situation is expected if the torsional frequency is smaller than the longitudinal one.

At any case, as previously explained, the longitudinal oscillations are responsible to cause the robot to swing back and forth in the sagittal plane along x-axis while torsional oscillations are responsible for up and down hopping movement in sagittal plane along z-axis. Therefore, having the two resonance frequencies close to each other should cause the robot to display behaviors of attempting to hop diagonally forward. On the other hand, if the two frequencies are clearly separated, there's a higher possibility to induce frequency close to the torsional or longitudinal frequency alone. In this case, it is reasonably more interesting to induce frequency close to the longitudinal frequency as it is supposed to cause the robot to have tendencies to purely slide forward instead of hop on its own place. Based on the characterization, the expected behavior when the robot is in upright and flat position should therefore be more suitable for normal and confined space respectively. It must of course be kept in mind that a robot's behavior will also depend on the environment, i.e. surface, as behavior is a result of the whole interaction among control input, body morphology and environments. At this stage of the study, we perform the experiments on a fixed surface as will be explained further in the next section.

3. Experiment Setup

In this section, we will describe in detail the design and implementation of the IUCBR for real world experiment. The objective of the experiment is to verify the assumption that the robot can adapt its behavior as desired while minimizing the required power by taking advantage of its shape changing ability. In this study, we consider the minimization of power instead of energy because the calculation of energy would also depend on how frequent there is a need to change the robot's shape and control input which depends on the application.

3.1. The Developed Robot and General Setup

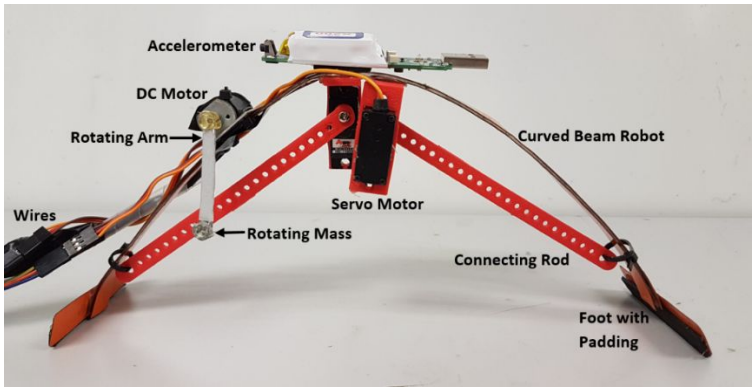

Figure 4. Inverted U-shape curved beam robot (IUCBR) whose components include DC motor, servo motors for shape changing ability and accelerometer to record the data.

Table 1. Mechanical parameters and their values of the real world Inverted U-shaped Curved Beam Robot (IUCBR).

Property	Value	Unit
Height of the robot	0.108, 0.124, 0.136	m
Length of the robot	0.183	m
Length of rotating mass	0.047	m
Mass of robot body	0.034	kg
Mass of DC motor with mount	0.022	kg
Mass of servo motor	0.017	kg
Mass of the accelerometer	0.040	kg
Rotating Mass	0.001	kg
Mass of IUCBR	0.127	kg

The inverted U-shaped curved beam robot (IUCBR) is made of compliant material in the form of an elastic metal beam referred as the body, attached to two horizontal metal strips called as the foot as shown in Fig. 4. The size, mass and relevant mechanical parameters are described in Table 1. The size of IUCBR is chosen as such to have a reasonable size for carrying out experiment easily on widely available standard wooden office tables. Additionally, the wooden surface of the table was also shown as adequately hard to demonstrate vibration-based locomotion (25; 26; 27). The curved beam robot is formed by cutting out two equal length long strips from electrical trunking, and acrylic foam tape with shear strength ≥ 200 gm/cm^2 is used to attach them. The final robot dimensions can be seen from Table 1.

We attach a brushless DC motor and a rotating mass on the rear leg of the robot. A Gulf Coast Data Concepts X200-4 USB impact accelerometer which is used to collect the data is placed at the topmost centre part of the robot body. Two Power HD-1160A miniature servos are placed under the

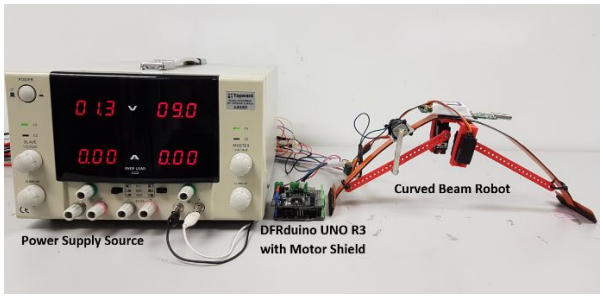

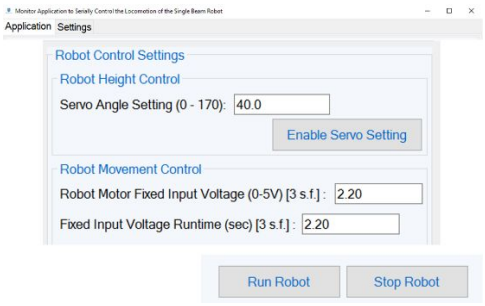

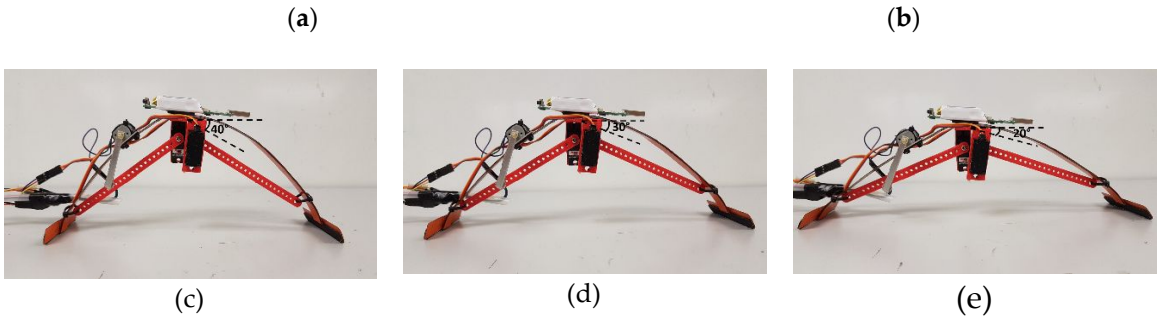

Figure 5. The complete real-world experimental setup. (a) & (b) show all the hardware components and software GUI to control the input to the IUCBR respectively. (c), (d) and (e) show the robot in different configurations namely 40, 30and 20. From application point of view, when it is necessary for the robot to go under potential confined spaces with different heights, shape changing ability enables the robot to achieve it. Also defined here is the configuration angle, which is measured as the angle between the horizontal and the shaft connected to servo motor.

joined strips in 3-D printed casing to hold them. The servo horns are replaced with 3-D printed shaft and is tied to the body near the foot. The presented structure is very easy and cheap to build, light weight and requires no complex control structure in order to move. The morphological design of the IUCBR is the main determinant of the robot locomotion in the presented design. The elasticity of steel strips makes the robot deformable and helps in its shape changing ability.

Based on the model explained in previous section and the discussed assumptions, we conduct experiment with the detailed experiment bench setup shown by Fig. 5. Fig. 5a exhibits the IUCBR with power supply and DFRduino board placed on a standard wooden office table with a size of 1.5'W x 6'L x 2.5'H. The top surface is laminated high pressured board with 18mm thickness. To measure the actual the input voltage and DC current across the terminals of DC motors, voltmeter and ammeter are connected in parallel and series respectively. Fig. 5b shows the software GUI to input the values for the used DC and servo motors, while Fig. 5c-5e shows the different configurations, i.e. shapes of the robot, through the use of the servo motors. The three values are chosen because they demonstrate different behaviors in different shapes.

Fig. 6 shows the IUCBR in motion for 30° configuration on experiment bench. The straight marking lines with spacing of 10 cm from each other served as a reference for measuring the distance.

Based on the research and analysis of previous research (25), it is easier to directly determine the relevant resonance frequencies rather than the involved stiffness in the model. Thus, similar to the procedure explained in (25), verifying equation (1) & (2) and (3) & (4), we determine the torsional and longitudinal frequencies by fixing the robot on the wooden table and gradually increase the voltage supplied to the DC motor that actuates the rotating mass while observing the vibration patterns of the robot when the robot is in the upright position, i.e. 40 configuration, and flat position, i.e. 20° configuration. Based on the observation, torsional vibration and longitudinal vibration of the IUCBR in upright position, induced by the rotating mass, has frequencies ω_{UT} = 23.4 Hz and ω_{UL} = 19.3 Hz respectively. While for the horizontal configuration of IUCBR, the torsional vibration and longitudinal vibration frequencies were recorded to be ω_{FT} = 27.2 Hz and ω_{FL} = 17.6 Hz respectively.

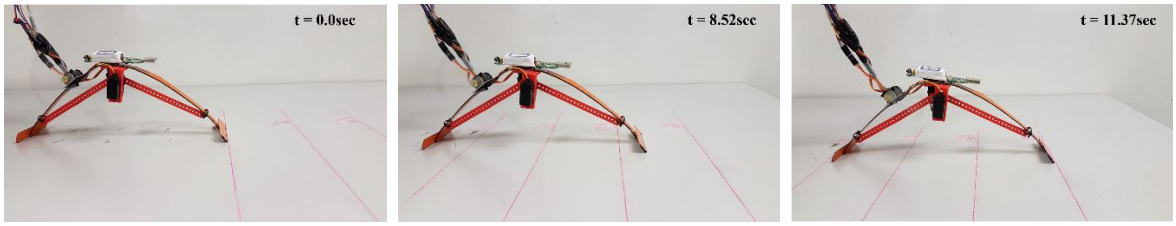

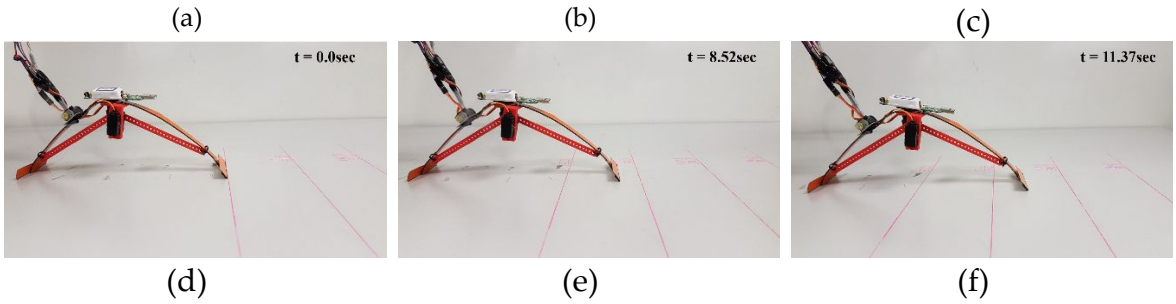

Figure 6. Snapshots of IUCBR in motion in 30 configuration on experiment table with four straight lines drawn at spacing of 10cmeach and top right value shows the time taken to reach that point from the starting point x = 0 at t = 0. The two rows differ in the input power supplied to the IUCBR which are 0.029W (V = 1.1V, I = 0.026A) and 0.078W (V = 1.7V, I = 0.046A) respectively. (a), (b) & (c) show the points reached by the robot at the same time but different supplied power.

The set of these values aligns with the derivation above, showing that if the longitudinal frequency is lower than the torsional one, then the two resonance frequencies are closer to each other when the robot is in the upright position compared to the flat position.

3.2. Experiment Procedure

In order to analyze the control-morphology space of the IUCBR, we investigate how its behavior is affected by both control inputs (voltage amplitude, V thus affecting driving frequency that actuates the rotating mass shown in Fig. 4) and morphology (in this context, shapes of the robot). To observe the behaviors, we measure the acceleration in different coordinates and then find the resultant magnitude

$$M = ||(PF_x, PF_z)|| \quad (3)$$

and arctan,

$$\gamma = \angle \arctan(PF_z, PF_x) \quad (4)$$

where PFx and PFz are values of power coefficients of the vibrations obtained from accelerometer and calculated by using FFT (Fast Fourier Transform) in x and z direction. Here, M is the magnitude of power coefficients and is measured from the ground. We ignore power coefficient in y axis because as already mentioned that the legs are wide enough such that it can be assumed that there's no significant difference in motion about the sagittal plane.

To analyze the robot's behavior in different shapes, we run 10 trials for the robot for each shape over a distance with a certain input voltage supplied to the DC motor. At each of this voltage V , we also record the supplied current I and thus calculate the power P supplied to the robot using P = V*I. To change the control input, we increase voltage V that rotates the rotating mass shown in Fig. 4 from 0.9V to 1.8V and as a result the current I from 0.020A to 0.055A. It means we gradually increase the power P from 0.018W to 0.097W. To change the shape, we use servo motor shown in Fig 4. The power required to actuate the servo motor is 0.008W. Both the change of control input and the change of shape happens instantaneously.

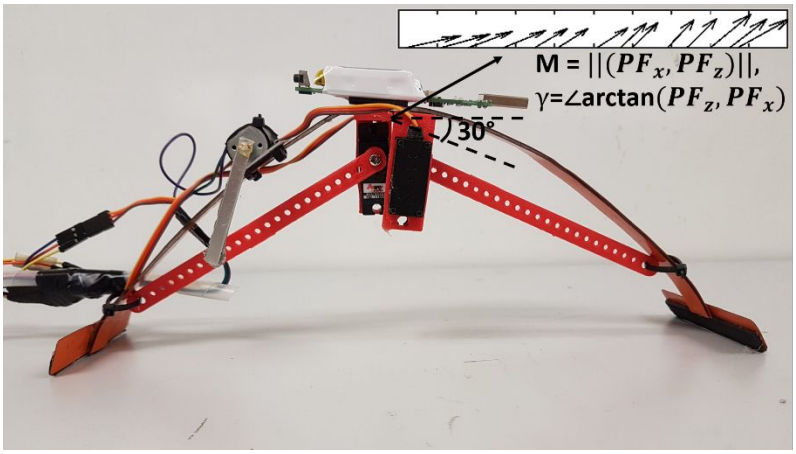

Figure 7. The schematic representation of the resultant magnitude M and its direction based on the value of the power coefficients PF_x & PF_z. Here the robot is in 30 configuration. The inset figure shows the resultant of magnitude and direction at the top of the robot corresponding to different input voltages.

By installing an accelerometer, we record the acceleration in the three axis and then use FFT to convert the data in frequency domain to get the power coefficients. The magnitude and phase of the obtained power coefficients of the resulting vibrational power PFx and PFz indicates the behavior of the robot as shown in Fig. 7. The shape of the robot is changed until all the three possible configurations (40, 30 and 20) are covered and the results for each shape can be compared. Here, the assumption is that because the change of the shape will change the values of the two resonance frequencies of the robot, it will be dominant in changing the robot's behavior while the required power to change the shape is minimized due to the use of elastic material.

The result will also be analyzed compared with the explained mathematical model, although we would like to emphasize that in real world experiment it is not possible to achieve a completely upright and flat shape such as assumed in the model. Nevertheless, as will be explained later, the results show adequately similarities with the model.

4. Experiment Result

The main goal of the experiment is to verify the main assumption that the robot's ability to change its shape will have significant role for adapting the robot's behavior while the required power for the purpose can be minimized. As explained in the previous section, changing the shape of the robot is supposed to lead to two main behaviors: when the robot is in upright position, its two resonance frequencies will be close to each other and will cause the robot to have tendencies to hop diagonally forward. On the other hand, when the robot is in flat position, it is possible to induce frequency close to the longitudinal frequency alone such that the robot will have tendencies to purely slide forward. For simplicity sake, the first behavior will be called "tendencies for hopping" or simply "hopping" and the second one will be called "tendencies for sliding" or simply "sliding" throughout the rest of the paper. While it is not the focus of the study, as explained in the previous section, from application point of view the two behaviors should be useful to deal with normal and confined spaces respectively.

The result and analysis will be presented based on the experiment procedure explained in the previous section. In the next sub-section, we will firstly present the result and analysis on how the change of control input and shape of the robot will change its behavior. Afterward, we will present the result and analysis that verifies whether and when the robot's ability to change its shape aside from its control input will have an important role to minimize the power required to change its behavior.

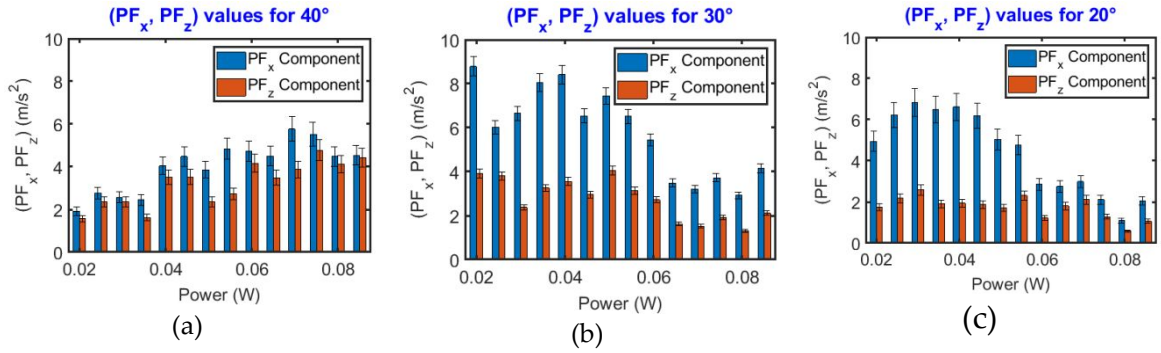

Figure 8. The magnitude of power coefficients PF_x and PF_z as recorded by the accelerometer, in the x and z axes respectively for the three configurations 40, 30 and 20, plotted against the input power P due to control input V and the resulting current I

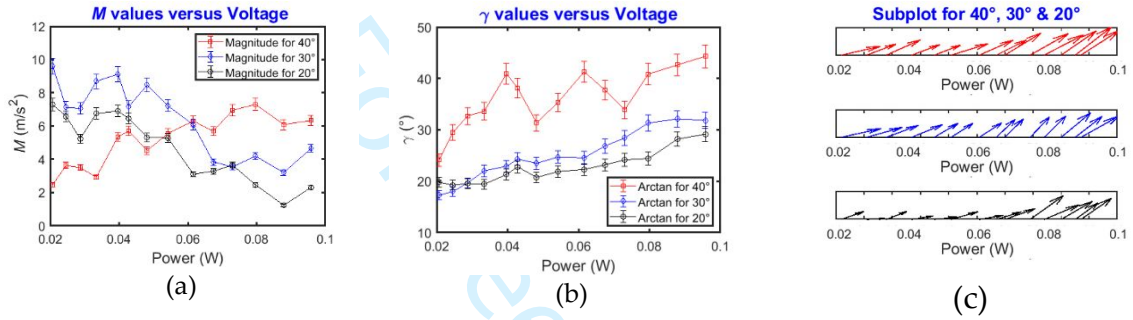

Figure 9. The magnitude and phase plot of the power coefficients of IUCBR over the entire input power range for 40 configurations based on the result shown in Fig. shown and explained in Fig. 9. (a) & (b) shows the line plot of magnitude and angle respectively while (c) is analogous to polar plot which graphically points the resultant magnitude, M, acting in a direction γ as experienced by IUCBR as shown and explained in Fig. 7.

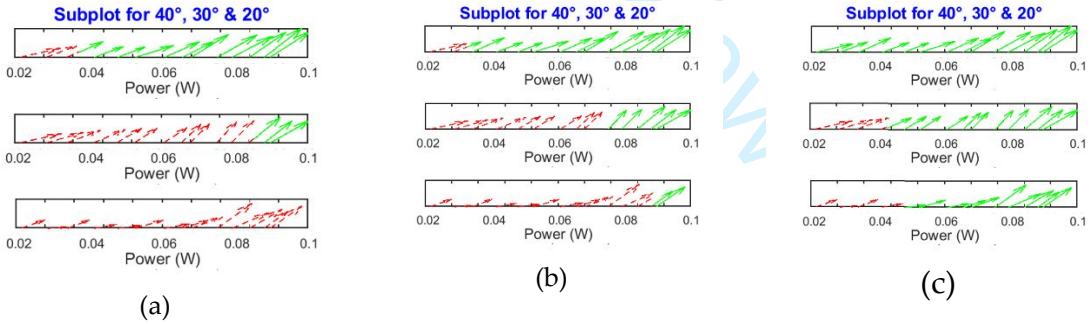

Figure 10. The polar plot shown in Fig. 9(c) can be used to indicate different behaviors of the robot by applying different thresholds to the γ = arctan (PFx; PFz) acts on the robot. Here, three thresholds are set at 30, 25 and 20 shown in Fig. 10. As a result, "sliding" behavior is shown by a dashed red line while "hopping" behavior is shown by a solid green line. When the robot is in different configuration of 40, 30 or 20, the dominant behavior will change.

4.1. Change of Behaviors

The experiment result in this section can be analyzed based on few figures, namely Fig. 8, 9 and 10. Fig. 8 shows the plot of two parameters to analyze the behavior of the robot. The first one is the power P used by the robot, resulting from the multiplication of voltage V as a control input that rotates the robot's DC motor and resulting current I. The second is the power coefficients of the robot's vibration, PFx and PFz, in x and y direction respectively. Fig. 8a shows the plot of these

parameters when the robot is in upright position, i.e. 40° configuration, while Fig. 8b and 8c shows the plot when the position is flatter, i.e. 30° and 20° configuration respectively. As can be seen, when the robot is in upright position, PFx and PFz occurs quite close to each other while in the case of 30 & 20 configuration they tend to be quite apart with PFx is significantly larger than PFz. The average difference between PFx and PFz for 40°, 30° & 20° configurations are 0.828 ± 0.598, 3.081± 1.205 and 2.615 ± 1.548 respectively. Also, the difference of these values between 40° configuration and the other two is statistically significant, while it is not between 30° & 20° configurations.

The shown pattern aligns with the basic idea and mathematical model explained in section Basic Concept and Relevant Mathematical Model. The model explains that when the robot is in upright position, the longitudinal and torsional resonance frequencies will be closed to each other and therefore the robot's oscillations will be dominant in both the x and z direction indicated by a close value between PFx and PFz shown in Fig. 8a. On the other hand, when the robot is flatter, it is possible to induce vibrations close to the longitudinal frequency, causing the robot to oscillate only along the x, i.e. forward, direction. The condition is indicated by a larger value of PFx in comparison with PFz shown in Fig 8b and 8c.

As also shown by Fig. 8 the change of control input, i.e. input voltage V that leads to different input power, does not change the pattern and therefore the effect of changing the shape is dominant. Probably the most important effect of changing the control input shown by the figure is in the case of upright position, i.e. 40° configuration, resonance of both torsional and longitudinal frequencies occurs at a moderately high value thus causing both PFx and PFz to reach their maximum value when the input power is approximately 0.07-0.08W. On the other hand, in a flatter position, i.e. 30° and 20° configurations, resonance of the longitudinal frequency occurs at a low value and causes PF to have a large value when the input power is approximately at 0.020.04W. The pattern is also expected by the model explained in Basic Concept and Relevant Mathematical Model section.

Having confirmed the hypothesized behavior, PF and PF are plotted into M and according to equation (19a) ad (19b). Fig 9a shows M plotted against power P given to the robot for all the three different shapes of the robot. Fig. 9b shows similar figure for γ. Finally, Fig. 9c is a polar plot that characterizes the robot's behavior through a graphical representation of the effect of magnitude M and angle to the robot's motion. It can be seen that for 20° configuration the magnitude decreases quite significantly at high control input V because the longitudinal and torsional frequencies occur at values which are farther from each other. Nevertheless, irrespective of the magnitude, is used to categorise the behavior which here is referred to as tendencies for "hopping" or "sliding" forward. Considering that the robot moves from left to right, it can be seen that when the robot is in upright position, the arrows shown in the polar plot tend to point diagonally upward. On the other hand, when the robot is in flat position, the arrows tend to point forward.

In order to clearly distinguish different behaviors for analysis purpose, several threshold values are applied to and Fig. 10 shows the definition of the robot's behavior based on Fig 9 by using the threshold values. To be more specific, in Fig 10a, it is defined that only when γ exceeds 30, the behavior can be categorized as "hopping", while the rest of the behaviors are defined as "sliding". The dashed and the solid line bars refers to sliding and hopping behavior respectively for 40°, 30° and 20° as shown. Fig. 10b and 10c show similar result with different definition of the threshold values, i.e. 25 and 20 respectively. From application point of view, the threshold values will depend on the environment, i.e. how vertically confined the space to be travelled by the robot. For the first value for the threshold used in this study, i.e. 30 , it can be seen from Fig. 10a that "hopping" is the dominant behaviors for 40 configuration, while "sliding" is the dominant behaviors for the other two as predicted by the model in section 2. When the threshold is lowered, then it will be easier for a behavior to be categorised as "hopping". Therefore, "hopping" becomes more dominant in the 30° and 20° configurations as well, as shown in Fig. 10b and 10c.

We also measure the average velocity at each shape over the entire input power range and the results are 0.060 m/s, 0.050 m/s, 0.048 m/s for 40 , 30 and 20 configuration respectively. As have been explained, the dominant behavior in the 40 configuration is tendencies for "hopping" while in 30 and 20 configuration is tendencies for "sliding" forward. The results shows that while the "sliding"

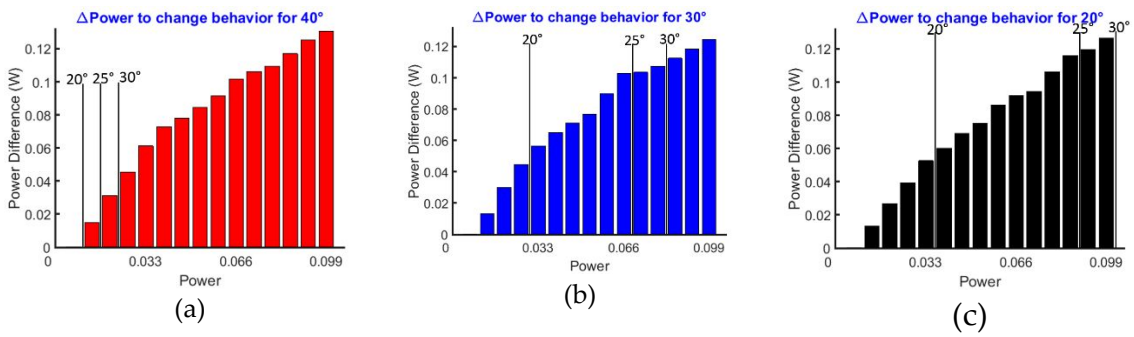

Figure 11. The bar plot showing the power difference for the IUCBR for three different configurations 40°, 30° and 20° plotted against the input power *P* based on the given control input *V* as explained in the Experiment Procedure section. Here, the term power difference refer to the increasingly input power *P* as the control input *V* is increased. The sliding and hopping behavior defined in Fig. 10. demarcated into separate regions by using transition lines for different threshold values of 30, 25 and 20.

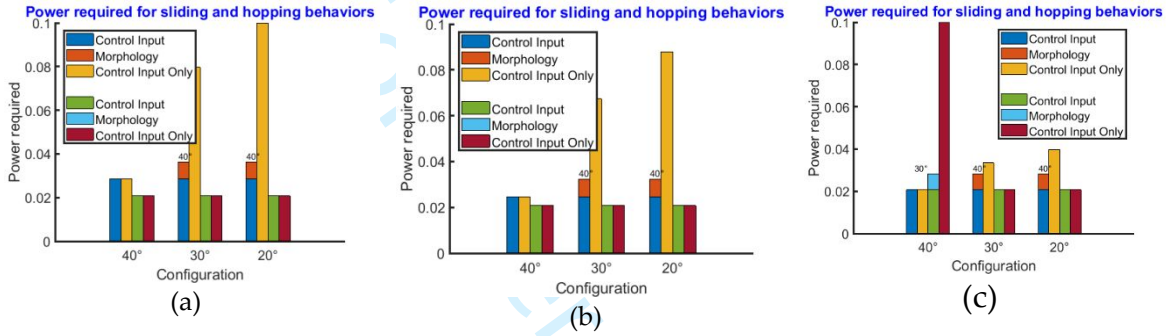

Figure 12. The required power (in Watts) by the IUCBR to change its behavior for each configuration with different thresholds of (a) 30, (b) 25 & (c) 20 respectively, that define hopping or sliding behavior. The first two bar on the left of configuration shows the required power to achieve "hopping" and the next two bar shows the required power to achieve "sliding". The robot always starts from its initial static behavior. The two adjacent bars for each configuration in the figure show the required power based on the two possibilities to achieve each behavior. The left one shows the required power if the robot is able to change both its shape and control input, while the right one shows the required power if the robot is only able to change its control input, i.e. it can only keep increasing its control input V without the ability to change to other possible configurations of 40, 30 & 20. The number on top of the stacked bars show the configuration that the robot needs to change its shape into, in order to minimize the power requirement to achieve the intended behavior.

behavior reasonably has lower velocity due to possible friction, the corresponding shape and direction of motion is more suitable or tasks like going under the confined space, a common challenge in soft robotics research.

Finally, based on Fig. 11, the power required to change the robot's behavior by changing the control input or shape can be analyzed as will be explained more in the next section.

4.1. Power Requirements for Changing Behaviors

In the previous section, it has been shown how the change of control input and shape affect the robot's behavior. In this section, more results will be presented to analyze whether and when it is possible for the robot to minimize the required power to change its behavior by taking advantage of its shape changing ability.

The first figure used to analyze the result is Fig. 11 that shows the plot of the power difference, ΔP, given to the robot, based on the control input V and resulting current I as explained in Experiment

Procedure subsection. The power difference is shown for each shape and, as can be seen, Fig. 11 aligns with Fig. 10 which show two behaviors of the robot, namely tendencies for "sliding" (dashed line) and "hopping" (solid line) forward, defined based on different threshold of γ shown in Fig. 7. It must also be noted that, as mentioned in the Experiment Procedure subsection, due to the elasticity of the robot's body, the change of the shape can simply be realized by a servomotor with a required power of 0.008W.

Based on Fig. 11, the power required, ΔP to change the robot's behavior can be analyzed through Fig. 12. To be more precise, Fig 12 shows the power required to achieve hopping (first two bars for a configuration) or sliding (next two bars of the same configuration), starting with zero control input V , for each of the three shapes for the three defined thresholds i.e. 30, 25, 20 respectively.

In Fig.12, the two horizontally adjacent bars, for a configuration, show the minimum power requirement to change the behavior assuming the robot can or cannot change its shape respectively. For example, Fig. 12a shows the required power to achieve hopping starting from zero control input V and therefore zero power P when the threshold is 30. In 40 configuration, referring to the top left figure of Fig. 11 it is meaningless for the robot to change its shape because the minimum power requirement is achieved if the control input, V , is simply increased until the robot switches its behavior from sliding to hopping i.e. having input power of 0.0287W or the first solid green bar shown in the figure. On the other hand, referring to the other figures of the first column in Fig 11, if the robot starts at 30 and 20configuration, having the ability to change shape is beneficial. Here, the minimum power requirement will be achieved if the control input, V , is increased up until certain level such that input power, P, equals to 0.0287W (the 3rd red bar shown in the figure) before the robot change its shape to 40 configuration. The total required power if the robot can change its shape is shown by the stacked bars, while the total required power if the robot cannot change its shape is shown by the standalone bar.

Observing all the sub-figures in Fig. 12, it can be seen that, to change its behavior, the power requirement if the robot can change its shape is always either equal or less than if the robot can only change its control input. In fact, seven out of eighteen studied conditions will have lower required power to change behavior, if the robot can change its shape. Therefore, it can be seen that the ability to change the shape leads to the desirable behaviors, with better power efficiency compared to when the robot solely relies on changing its control input.

5. Discussion

This article presents the development and analysis of a locomoting robot with shape changing ability that relies on the ability of elastic beams to deform and vibrate. It has been shown both analytically and experimentally that, through a proper use of the elastic materials and the vibration dynamics of the robot, the shape adaptation of the robot leads to desirable behaviors with better power efficiency compared to when the robot solely relies on changing its control input. The approach shown motivates investigation of new approaches to efficiently change robots' behaviors by changing their shape or morphology, instead of solely relying on changing the robots' control inputs. As also explained in the introduction section, the approach is motivated by an increasing interest in using soft and elastic materials for robotic systems. To be more specific, in this particular work, our approach is to relate the shape of the robot with its resonance frequencies to determine how the robot can adapt its behavior by changing its shape while minimizing the required power.

Conventional methods to change a robot's behavior by changing its control input brings about a lot of interests on high level programming of a robot with a fix body morphology, which is commonly applied in rigid robots (52; 53). On the other hand, the approach shown encourages investigation of approaches to change robots' behavior by changing their shape and morphology. While the idea that the morphology of a robot can facilitate control has been argued in previous studies (2; 3; 5; 54), to the best of our knowledge this work is the first that systematically shows that a robot's shape adaptation, as an example of morphological adaptation, can lead to the desired behaviors with better power efficiency than when the robot only relies on its control input. We have also argued that the use of elastic materials is the key factor that enables the robot to easily change its

shape with a minimum amount of power. In this work, we rely on the use of elastic beam and resonance frequencies to determine the change of shape that will lead to significantly different behaviors with minimum power. While here we use a curved beam robot with inverted U-shaped but the results can generalize to other shapes as long as the relationship between the shape and the resulting resonance frequencies is clarified. For instance, in (28), the relationship between the resonance frequencies and the shape of the robot was explained in a C-shaped hopping robot although the robot did not have any mechanism yet to adjust its own shape. Moreover, a systematic study on whether the changes of morphology leads to significantly different behaviors while the required power is minimized can also be explored in other methods that enable adaptive morphology such as morphing wings in flying robot or morphing wheels in a ground mobile robot (5). We believe that a proper use of soft and elastic materials should be the key factor to minimize the required power to change the robot's morphology.

In the analysis of the robot behaviors, we use a combination of simple linear and rotational springs and even with this simplified model, the simulation and experimental results that explain the behaviors match reasonably well. Nevertheless, as mentioned in the last paragraph in the Basic Concept and Relevant Mathematical Model section, it must also be kept in mind that a behavior will always depend on the whole interaction among its control input, body morphology and environments. In this context, the appendix shows the ground interaction model that we used and verified in our previous work (26). The vertical ground interaction forces are approximated by nonlinear spring-damper interactions and the horizontal forces are calculated by a sliding stiction model. The vertical and horizontal ground reaction forces depend on several parameters such as the friction and damping coefficients which will depend on the environment. While the calculation of the resonance frequencies is not directly related with the model, the effect of the ground interaction forces is encapsulated in the power coefficients recorded by the accelerometer (PFx and PFz along the x and z direction respectively). In this study, while the effect of the ground reaction forces is already incorporated, it is not explicitly modelled. Therefore, a more detailed explanation of how ground surface interaction can be modelled as part of a future work is mentioned in the Appendix section. In this paper, the motion of the robot is considered in two direction, along x and z-axes, which is measured using an accelerometer during the motion and the values are used to calculate PFx and PFz. Thus, PFx and PFz contain the information of ground reaction force although it's not explicitly modelled. For example, if the surface is not sufficiently hard and the vertical reaction force is low, it may lower down the value of the power coefficients along the z direction even if the robot is in an upright position. While in this work we choose a wooden surface where the effect of different resonance frequencies has been shown to be significant (25; 26; 27); which showed some initial works that discuss the importance of morphology and energy efficiency, it is interesting to perform experiments in other types of surfaces as a future work. Aside from that, it will also be interesting to model the relationship between resonance frequency and the dynamic motion of the robot, such as explained for other types of motion like swimming motion (55). It is also possible to relate the optimum energy with resonance frequency (56), which is not the focus of this paper. The main goal of this paper is to explain and demonstrate that adaptive behavior can be achieved in a more power efficient manner through the use of a shape changing elastic body.

Last but not last, there are surely several limitations of this work. Here, we only explore shape changing ability enabled by the elastic body while there are also other approaches to realize morphological adaptation in a robot. In our previous works, we have also investigated other parameters, i.e. different types of morphology, such as different shapes, leg configurations and masses. For example, we have shown that the increasing value of the rotating mass would increase the centripetal force that drives the robot's motion (25; 26). However, unlike shape changing mechanism, it may not be feasible to have a mechanism that enables the robot to adjust its own mass and quantify the required power. Another interesting example of morphological adaptation will be stiffness changing ability. In the mathematical model shown in the appendix, the effect of different stiffness for the developed robot is also outlined. For instance, the larger the torsional stiffness of the robot, the torsional resonance frequency of the robot will become larger as well. Nevertheless,

enabling the robot to adjust its own stiffness is far from trivial either (5; 57) and therefore at this stage we focus on shape changing ability as an example of morphological adaptation. All in all, to the best of our knowledge, this work is the first that systematically shows how shape changing ability enables the robot to adapt its behavior while minimizing the required power compared to when the robot solely relies on changing its control input through a proper use of elastic materials.

6. Conclusions and Future Work

The advancement in the field of soft robotics that studies robots that can achieve deformability through their inherent material properties or structural compliance opens new perspectives on how robots should change their behaviors. Nevertheless, this type of robots generally have quite complex dynamics and thus it is difficult to substantiate whether and when it is beneficial for the robot in terms of cost such as the required power to adapt its behavior by taking advantage of its shape changing ability. In this paper, we have presented the development of a vibration based locomoting robot made of elastic materials with structural compliance and analyzed the power requirements for changing its behavior. We have shown through mathematical modelling and real-world experiment that the robot will adapt its behavior as desired when it changes its shape. Moreover, due to the elasticity of the body, the power required to change the shape of the robot is minimized. In this work, we have also analyzed whether and when it is possible for the robot to minimize the required power to change behavior by taking advantage of its shape changing ability. In our experiment setting, it is shown that in order to change the robot's behavior, the power requirement if the robot can change its shape is always either equal or less than if the robot can only change its control input. In other words, the ability to change the shape enables the robot to adapt its behaviors, with better power efficiency compared to when the robot solely relies on changing its control input.

As discussed in the previous section, the proposed concept and design approach encourages alternative research directions as compared to the classical approach of changing a robot's behavior, i.e. by changing its control input. The classical approach, for example, brings about a lot of interests on high level programming of a robot's behavior with a predefined body. On the other hand, the approach shown motivates investigation of new approaches to change robots' behaviors by changing their shape and morphology, while being able to substantiate that the change of the robot's shape will lead to the desired behaviors.

Nevertheless, as explained in more details in the discussion section, there are also a number of limitations to the current study which can be explored in the future. For example, in this current work, we only explore shape changing ability enabled by the robot's elastic body while there are other possible approaches for morphological adaptation such as varying the robot's stiffness. The proposed design alone also has some other parameters that can be varied to see how they change the robot's behavior, such as the mass and size of the robot. It must also be kept in mind that a robot's behavior is essentially its dynamics resulting from the interaction among its control input, body morphology and environment. Therefore, it will also be interesting to perform experiments on different environments such as different surfaces and see how they affect the robot's behavior, as well as to explicitly model the effect of the ground reaction forces. Last but not least, another possible future work is the investigation of how to embed the robot with autonomous decision-making capability on when it's supposed to change its behavior by changing its shape.

Conflicts of Interest: The authors declared no potential conflicts of interest with respect to research, authorship, and/or publication of this article.

Funding: The authors acknowledge the support of the FRGS Grant (Project no: FRGS/1/2017/ICT02/MUSM/03/3) provided by the Ministry of Higher Education (MOHE), Malaysia, and the School of Engineering Seed Funding (2016), Monash University Malaysia. Shiv Katiyar is supported by Merit Scholarship Monash University Malaysia.

Acknowledgments: The authors would also like to mention and thank Maninda Andradi for his contribution in developing the basic structure of the IUCBR, Ghopy Kandasamy for designing the GUI used to control the input voltage, Eranda Kulatunga, Md. Mustafizur and Sheng Hong Chuwa for their assistance in data collection.

Appendix A: Mathematical Modeling

To analytically determine the effect of torsional and longitudinal resonance frequencies in the two configurations as shown in Fig. 3, we use Lagrangian method. Consider the mass spring system with massless & inertia less link and inertia less point mass as shown in the Fig. 3. The following combination of the kinetic and potential energies (T and V respectively) can be written as:

$$L \equiv T - V \tag{5}$$

and is called the Lagrangian L of the system. Based on L, the Euler-Lagrange equation which can be used to derive the equation of motion is written as:

$$\frac{d}{dt}\left(\frac{\partial L}{\partial \dot{q}}\right) - \frac{\partial L}{\partial q} = F \tag{6}$$

where q represents the possible generalized coordinates and the conservative forces are assumed to be zero. Furthermore, based on the left figure of Fig. 3, the kinetic energy, T can be broken up into the radial and tangential parts, so we have:

$$T = \frac{1}{2}m\dot{l}^2 + \frac{1}{2}m(l\dot{\beta})^2 \tag{7}$$

The potential energy V comes from both gravity, $mgl\cos\beta$, and the two springs and thus V can be written as:

$$V = mgl\cos\beta + 2 * \frac{1}{2}k_L l^2 + 2 * \frac{1}{2}k_\beta \beta^2 \tag{8}$$

Therefore, by using (5), the Lagrangian, L becomes:

$$L \equiv \frac{1}{2}m\dot{l}^2 + \frac{1}{2}m(l\dot{\beta})^2 - mgl\cos\beta - 2 * \frac{1}{2}k_L l^2 - 2 * \frac{1}{2}k_\beta \beta^2 \tag{9}$$

As the problem involves more than one generalized coordinate, i.e. l and β, equation (12) & (13) must be applied for each coordinate. Differentiating (9) with respect to β, i.e. l is assumed to be constant, and with l, assuming β to be constant the homogeneous part of the Euler-Lagrange equation can be written as shown in (14) and (17).

$\frac{d}{dt}\left(\frac{\partial L}{\partial \dot{\beta}}\right) - \frac{\partial L}{\partial \beta} = ml^2\ddot{\beta} - mgl\sin\beta + 2k_\beta\beta$	$\frac{d}{dt}\left(\frac{\partial L}{\partial \dot{l}}\right) - \frac{\partial L}{\partial l} = m\ddot{l} + mg\cos\beta + 2k_L l - ml\dot{\beta}^2$	(10)

Similarly, when the robot is in flat position, the Lagrangian L and the relevant angle (90° - β), defined as being measured in anti-clockwise direction from the horizontal line.

$$L \equiv \frac{1}{2}m\dot{l}^2 + \frac{1}{2}m(l\dot{\beta})^2 - mgl\sin(90° - \beta) - 2 * \frac{1}{2}k_L(l)^2 - 2 * \frac{1}{2}k_\beta \beta^2 \tag{11}$$

Differentiating with respect to the two variables, i.e. l and β, for each coordinate separately the homogeneous part of the Euler-Lagrange equation can be written as shown in (14a) and (14b).

$\frac{d}{dt}\left(\frac{\partial L}{\partial \dot{\beta}}\right) - \frac{\partial L}{\partial \beta} = ml^2\ddot{\beta} - mgl\sin\beta + 2k_\beta\beta$	$\frac{d}{dt}\left(\frac{\partial L}{\partial \dot{l}}\right) - \frac{\partial L}{\partial l} = m\ddot{l} + mg\cos\beta + 2k_L l - ml\dot{\beta}^2$	(12)

For IUCBR in the upright and the flat position we assume $\beta \approx 0$, therefore $\sin\beta \approx \beta$ and when $\beta \approx 90$ then $\sin\beta \approx 1$

$ml^2\ddot{\beta} - mgl\beta + 2k_\beta\beta = 0$	$ml^2\ddot{\beta} + mgl\beta + 2k_\beta\beta = 0$	13

The general form of the equation of motion involving the torsional frequency ω_β is as follows:

$$\ddot{\beta} + \omega_{\beta}^2\beta = 0 \quad 14$$

By comparing the above two equations, we obtain the torsional resonance frequency as:

$\omega_{UT} = \sqrt{\frac{2k_\beta - mgl}{ml^2}}$	$\omega_{FT} = \sqrt{\frac{2k_\beta + mgl}{ml^2}}$	15

Similarly, applying (13) with respect to l, i.e. ωβ is assumed to be constant, the homogeneous part of the Euler-Lagrange equation can be written as shown in (20a) and (20b).

$m\ddot{l} + 2k_L(l) = 0$	$m\ddot{l} + mg\beta + 2k_L(l) = 0$	16

The general form of the equation of motion involving the longitudinal frequency ω_β is as follows:

$$\ddot{l} + \omega_L^2 l = 0 \quad 17$$

therefore, the longitudinal resonance frequency is of the form

$$\omega_{UL} = \omega_{FL} = \sqrt{\frac{2k_L}{m}} \quad 18$$

Appendix B: Ground Interaction Model

The vertical ground interaction forces can be approximated by nonlinear spring-damper interactions where the horizontal forces are calculated based on a sliding-stiction model (26). In the model, the switches between sliding and stiction depends on whether the velocity of the foot is lower or higher than a specified limit which is determined by the sliding and stiction friction coefficients, μ_{slide} and μ_{stick}, respectively. All in all, the vertical and horizontal ground reaction forces, G_{yi} and G_{xi} respectively, can be calculated as:

$$G_{yi} = -a|\dot{y}_{ci}|^3(1 - b\dot{y}_{ci}) \quad 19$$

$$G_{xi} = \begin{cases} \mu_{\text{slide}} G_{yi} \dfrac{\dot{x}_{ci}}{|\dot{x}|_{ci}}, & if\ F_{xci} > \mu_{\text{stick}} G_{yi} \dfrac{\dot{x}_{ci}}{|\dot{x}_{ci}|} \\ F_{xci}, & \text{otherwise} \end{cases} \quad 20$$

where the horizontal velocity and vertical distance of the contact point, *i* from the ground surface are denoted as $\dot{x}_{ci}$ and $\dot{y}_{ci}$ respectively, and the computed force at the foot contact point, *i* is denoted as F_{xci} and the friction coefficients (μ_{slide}, μ_{stick}) in the model depend on the environment.

References

1. Dickinson, Michael H and Farley, Claire T and Full, Robert J and Koehl, MAR and Kram, Rodger and Lehman, Steven How animals move: an integrative view Science 288(5463):pages 100–106. American Association for the Advancement of Science, 2000.
2. Pfeifer, Rolf and Bongard, Josh. How the body shapes the way we think: a new view of intelligence. MIT press, 2006.

3. Pfeifer, Rolf and Lungarella, Max and Iida, Fumiya. Self-organization, embodiment, and biologically inspired robotics. In science, 318(5853):pages 1088–1093. American Association for the Advancement of Science, 2007.
4. Yu, Xiaoxiang and Nurzaman, Surya Girinatha and Culha, Utku and Iida, Fumiya. Soft robotics education Soft Robotics, 1(3):202–212, 2014.
5. Stefano Mintchev and Dario Floreano. Adaptive morphology: A design principle for multimodal and multifunctional robots. IEEE Robotics & Automation Magazine, 23(3):42–54, 2016.
6. Fumiya Iida and Surya G Nurzaman. Adaptation of sensor morphology: an integrative view of perception from biologically inspired robotics perspective. Interface Focus, 6(4):20160016, 2016.
7. Culha, Utku and Wani, Umar and Nurzaman, Surya G and Clemens, Frank and Iida, Fumiya. Motion pattern discrimination for soft robots with morphologically flexible sensors. Intelligent Robots and Systems (IROS 2014), 2014 IEEE/RSJ International Conference on, pages 567–572. IEEE, 2014.
8. Liyu Wang, Surya G. Nurzaman, and Fumiya Iida. Softmaterial robotics. Foundations and Trends in Robotics, 5(3):191–259, 2017.
9. Wang, Liyu and Iida, Fumiya. Deformation in soft-matter robotics: A categorization and quantitative characterization IEEE Robotics & Automation Magazine 22,3. 2015.
10. K. Kotay and D. Rus. Locomotion versatility through selfreconfiguration. Robot. Autom. Syst., vol. 26, pp. 217–232, 1999.
11. W. M. Shen, M. Krivokon, H. Chiu, J. Everist, M. Rubenstein, and J. Venkatesh. Multimode locomotion via SuperBot reconfigurable robots. Autonomous Robots, vol. 20, no. 2, pp. 165–177, 2006.
12. M. Yim, D. G. Duff, and K. D. Roufas. Modular self reconfigurable robot systems. IEEE Robot. Automat. Mag., vol. 14, no. 1, pp. 43–52, Mar. 2007.
13. Sproewitz, Alexander and Billard, Aude and Dillenbourg, Pierre and Ijspeert, Auke Jan. Roombots-mechanical design of self-reconfiguring modular robots for adaptive furniture IEEE International Conference on Robotics and Automation 4259– 4264, 2009.
14. Surya G Nurzaman, Fumiya Iida, Cecilia Laschi, Akio Ishiguro, and Robert Wood. Soft robotics – Technical Committee Spotlight. IEEE Robotics & Automation Magazine, 20(3):24–95, 2013.
15. Surya G Nurzaman, Fumiya Iida, Laura Margheri, and Cecilia Laschi. Soft robotics on the move: scientific networks, activities, and future challenges. Soft Robotics 1 (2), 154-15, 2014.
16. Cecilia Laschi and Matteo Cianchetti. Soft robotics: new perspectives for robot bodyware and control. Frontiers in Bioengineering and Biotechnology, 2:3, 2014.
17. Daniela Rus and Michael T Tolley. Design, fabrication and control of soft robots. Nature, 521(7553):467–475, 2015.
18. Laschi, Cecilia and Mazzolai, Barbara and Cianchetti, Matteo. Soft robotics: Technologies and systems pushing the boundaries of robot abilities. Sci. Robot., 1:1, EAAH 3690 2016.
19. J. R. Amend, E. Brown, N. Rodenberg, H. M. Jaeger, and H. Lipson. A positive pressure universal gripper based on the jamming of granular material IEEE Trans. Robot., vol. 28, no. 2, pp. 341–350, Apr. 2012.
20. Erik Steltz, Annan Mozeika, Nick Rodenberg, Eric Brown, and Heinrich M Jaeger. Jsel: Jamming skin enabled locomotion. In Intelligent Robots and Systems, 2009. IEEE/RSJ International Conference on, pages 5672–5677. IEEE, 2009.
21. Filip Ilievski, Aaron D. Mazzeo, Robert F. Shepherd, Xin Chen and George M. Whitesides. Soft Robotics for Chemists Angewandte Chemie Journal of German Chemical Society 2011.
22. Robert F Shepherd, Filip Ilievski, Wonjae Choi, Stephen A Morin, Adam A Stokes, Aaron D Mazzeo, Xin Chen, Michael Wang, and George M Whitesides. Multigait soft robot. Proceedings of the National Academy of Sciences, 108(51):20400–20403, 2011.
23. Kyunam Kim, Adrian K Agogino, Deaho Moon, Laqshya Taneja, Aliakbar Toghyan, Borna Dehghani, Vytas SunSpiral, and Alice M Agogino. Rapid prototyping design and control of tensegrity soft robot for locomotion. In Robotics and Biomimetics (ROBIO), 2014 IEEE International Conference on, pages 7–14. IEEE, 2014.
24. Rieffel, John A and Valero-Cuevas, Francisco J and Lipson, Hod. Morphological communication: exploiting coupled dynamics in a complex mechanical structure to achieve locomotion Journal of the royal society interface, The Royal Society.7, 45. 2010.
25. Murat Reis and Fumiya Iida. An energy-efficient hopping robot based on free vibration of a curved beam. IEEE/ASME Transactions on Mechatronics, 19(1):300–311, 2014.

26. Murat Reis, Xiaoxiang Yu, Nandan Maheshwari, and Fumiya Iida. Morphological computation of multi-gaited robot locomotion based on free vibration. Artificial life, 19(1):97–114, 2013.
27. Nurzaman, SG and Yu, Xiaoxiang and Kim, Yongjae and Iida, Fumiya. Goal-directed multimodal locomotion through coupling between mechanical and attractor selection dynamics. Bioinspiration & biomimetics, 10,2. IOP Publishing 2015.
28. Shintake, Jun and Cacucciolo, Vito and Floreano, Dario and Shea, Herbert. Soft robotic grippers Advanced Materials 30(29):1707035, 2018.
29. A. T. Asbeck, S. M. M. De Rossi, I. Galiana, Y. Ding, and C. J. Walsh. Stronger, smarter, softer: next-generation wearable robots. IEEE Robotics &Automation Magazine, 21(4):22–33, December 2014.
30. Shahid, Talha and Gouwanda, Darwin and Nurzaman, Surya G and Alpha A. Gopalai. Moving toward soft robotics: A decade review of the design of hand exoskeletons Biomimetics, Multidisciplinary Digital Publishing Institute. 3, 3. 2018.
31. M. Cianchetti, T. Ranzani, G. Gerboni, T. Nanayakkara, K. Althoefer, P. Dasgupta, and A. Menciassi. Soft robotics technologies to address shortcomings in today's minimally invasive surgery: the stiff-flop approach. Soft Robotics, 1(2):122–131, June 2014.
32. Sadati, SM Hadi and Noh, Yohan and Naghibi, S Elnaz and Kaspar, Althoefer and Nanayakkara, Thrishantha Stiffness control of soft robotic manipulator for minimally invasive surgery (MIS) using scale jamming International Conference on Intelligent Robotics and Applications 141–151, 2015.
33. Rieffel, John and Mouret, Jean-Baptiste. Adaptive and resilient soft tensegrity robots Soft robotics, Mary Ann Liebert, Inc. 140 Huguenot Street, 3rd Floor New Rochelle, NY 10801 USA, 5:3, 318–329.2018
34. B¨ohm, Valter and Zimmermann, Klaus. Vibration-driven mobile robots based on single actuated tensegrity structures in IEEE International Conference on Robotics and Automation, 5475–5480. 2013.
35. Schorr, Philipp and B¨ohm, Valter and Zentner, Lena and Zimmermann, Klaus. Design of a Vibration Driven Motion System Based on a Multistable Tensegrity Structure in International Conference on Informatics in Control, Automation and Robotics, Springer, 302–317, 2018.
36. Djen Timo Kuhnel and Tim Helps and Jonathan Rossiter. Kinematic Analysis of VibroBot: A Soft, Hopping Robot with Stiffness - and Shape Changing Abilities In Front. Robotics and AI, 2016.
37. Miyashita, Shuhei and Guitron, Steven and Li, Shuguang and Rus, Daniela. Robotic metamorphosis by origami exoskeletons Science Robotics, eaao4369, 2017 Science Robotics.
38. Felton, Samuel M.and Lee Dae-Young and Cho, Kyu-Jin and Wood, Robert J. A passive, origami-inspired, continuously variable transmission IEEE International Conference on Robotics and Automation (ICRA), 2014.
39. Liu, Ke and Wu, Jiangtao and Paulino, Glaucio H and Qi, H Jerry. Programmable deployment of tensegrity structures by stimulus-responsive polymers Scientific reports, Nature Publishing Group, 7, 1 2017.
40. Nurzaman, Surya G and Culha, Utku and Brodbeck, Luzius and Wang, Liyu and Iida, Fumiya. Active sensing system with in situ adjustable sensor morphology PLoS One, Public Library of Science, 8, 12. 2013.
41. Hawkes, Elliot W and Blumenschein, Laura H and Greer, Joseph D and Okamura, Allison M A. Soft robot that navigates its environment through growth Science Robotics, 2, 8. 2017.
42. B.E. Schubert and D. Floreano. Variable stiffness material based on rigid low-melting-point-alloy microstructures embedded in soft poly (dimethylsiloxane) (PDMS) RSC Advance., vol. 3, no. 46, pp.24671–24679,2013.
43. Meng, Harper and Li, Guoqiang. A review of stimuliresponsive shape memory polymer composites Polymer Elsevier vol.54, no.9,pp.2199–2221,2013.
44. N.G.Cheng, A.Gopinath, L.Wang, K.Iagnemma, and A.E.Hosoi. Thermally tunable, self-healing composites for soft robotic applications Macromol. Mater. Eng.,vol.299,no.11,pp.1279–1284,Nov. 2014.
45. C. Majidi and R.J.Wood. Tunable elastic stiffness with micro confined magnetorheological domains at low magnetic field Appl. Phys. Lett., vol.97,no.16,pp.2010–2012,2010.
46. F. Corucci, M. Calisti, H. Hauser, and C. Laschi. Evolutionary discovery of self-stabilized dynamic gaits for a soft underwater legged robot in Proc. 2015 Int. Conf. Adv. Robot. IEEE, 2015, pp. 337–344.
47. D. Owaki, M. Koyama, S. Yamaguchi, S. Kubo, and A. Ishiguro. A two-dimensional passive dynamic running biped with knees in Proc. 2010 IEEE Int. Conf. Robot. Autom. IEEE, 2010, pp. 5237–5242.
48. Yoichi Masuda, Keisuke Naniwa, Masato Ishikawa, and Koichi Osuka. Weak Actuators Generate Adaptive Animal Gaits without a Brain IEEE International Conference on Robotics & Biomimetics 2017.

49. Hideyuki Ryu, Yoshihiro Nakata, Yutaka Nakamura, Hiroshi Ishiguro. Adaptive Whole-Body Dynamics: An Actuator Network System for Orchestrating Multijoint Movements IEEE Robotics & Automation Magazine. 23, 3. 2016.
50. H. Hauser and F. Corucci. Morphosis—Taking morphological computation to the next level in Proc. Soft Robot., Trends, Appl. Challenges. Springer, 2017, pp. 117–122.
51. Garrad M, Rossiter J, Hauser H. Shaping Behavior With Adaptive Morphology. IEEE Robotics and Automation Letters. 2018 Feb 19;3(3):2056-62.
52. Bascetta, Luca and Rocco, Paolo. Revising the robust-control design for rigid robot manipulators. IEEE Transactions on Robotics, 26: 1, 180–187. 2009.
53. Giusti, Andrea and Althoff, Matthias. Ultimate robust performance control of rigid robot manipulators using interval arithmetic. 2016 American Control Conference (ACC), 2995– 3001. 2016.
54. M¨uller, Vincent C and Hoffmann, Matej. What is morphological computation? On how the body contributes to cognition and control. Artificial life, MIT Press, 23:1, 1–24. 2017.
55. Carbajal, Juan Pablo, Rafael Bayma, Marc Ziegler, and Zi-Qiang Lang. "Modeling and frequency domain analysis of nonlinear compliant joints for a passive dynamic swimmer." arXiv preprint arXiv:1108.3206 (2011).
56. Katiyar, Shiv, Ghopy Kandasamy, Eranda Kulatunga, Md Mustafizur, Fumiya Iida, and Surya G. Nurzaman. "Morphological adaptation in an energy efficient vibration-based robot." In 2018 IEEE International Conference on Robotics and Automation (ICRA), pp. 1575-1582. IEEE, 2018.
57. Manti, Mariangela and Cacucciolo, Vito and Cianchetti, Matteo. Stiffening in soft robotics: A review of the state-of-the-art IEEE Robotics & Automation Magazine, 23:3, 93–106. 2016.

Shiv A. Katiyar received his master's degree from Indian Institute of Information Technology-Allahabad, India in 2014. He is currently working towards his doctoral degree from Monash University Malaysia since 2016. Before enrolling for PhD, he gained industrial experience as a Software Engineer with Verizon India from 2014 to 2016. His primary research interest includes bio-inspired robotics and soft robotics.

Darwin Gouwanda received his undergraduate degree in Mechatronics Engineering and his PhD in Biomedical Engineering from Monash University. He is currently a senior lecturer at School of Engineering, Monash University Malaysia. His primary research interests include motion analysis, wearable devices and rehabilitation robots.

Fumiya Iida has been a university reader at the University of Cambridge since 2018. Previously he was an assistant professor for bio-inspired robotics at ETH Zurich (2009-2014) and a lecturer at Cambridge (2014-2018). He received his bachelor and master's degrees in mechanical engineering at Tokyo University of Science (Japan, 1999), and Dr. sc. nat. in Informatics at the University of Zurich (2006). In 2004 and 2005 he was also engaged in biomechanics research of human locomotion at Locomotion Laboratory, University of Jena (Germany). His research interests include biologically inspired robotics, embodied artificial intelligence, and biomechanics, where he was involved in several research projects related to dynamic legged locomotion, navigation of autonomous robots, and human-machine interactions.

Surya Nurzaman is a Senior Lecturer at the Mechanical Engineering Discipline, School of Engineering, Monash University Malaysia. He obtained his Ph.D. degree from Osaka University, Japan in 2011 and was a Research Fellow in Osaka University, ETH Zürich and University of Cambridge until 2015. Prior to coming to Japan in 2007, he finished his Bachelor and Master degrees in Institute of Technology Bandung, Indonesia, and worked as a technology consultant in Accenture for a few years, accomplishing various projects in Indonesia, Malaysia, Singapore and the United States. His research interests include soft robotics, bio-inspired robotics, dynamical systems and embodied intelligence. He has also been serving as the Newsletter Editor-in-Chief of the IEEE RAS Technical Committee on Soft Robotics since 2013.